A FRAMEWORK FOR THE DETECTION OF ACUTE RENAL REJECTION WITH DYNAMIC CONTRAST ENHANCED MAGNETIC RESONANCE IMAGING

Aly Farag[1], *Ayman El-Baz*[1], *Seniha E. Yuksel*[1], *Mohamed A. El-Ghar*[2] , *and Tarek Eldiasty*[2]

[1]CVIP Lab., ECE Dept.
University of Louisville, Louisville, KY, USA

[2]Urology and Nephrology Department
University of Mansoura, Mansoura, Egypt

ABSTRACT

Acute rejection is the most common reason of graft failure after kidney transplantation, and early detection is crucial to survive the transplanted kidney function. In this paper we introduce a new approach for the automatic classification of normal and acute rejection transplants from Dynamic Contrast Enhanced Magnetic Resonance Imaging (DCE-MRI). The proposed algorithm consists of three main steps; the first step isolates the kidney from the surrounding anatomical structures by evolving a deformable model based on two density functions; the first function describes the distribution of the gray level inside and outside the kidney region and the second function describes the prior shape of the kidney. In the second step, nonrigid-registration algorithms are employed to account for the motion of the kidney due to patient breathing, and finally, the perfusion curves that show the transportation of the contrast agent into the tissue are obtained from the cortex and used in the classification of normal and acute rejection transplants. Applications of the proposed approach yield promising results that would, in the near future, replace the use of current technologies such as nuclear imaging and ultrasonography, which are not specific enough to determine the type of kidney dysfunction.

1. INTRODUCTION

In the United States, approximately 12000 renal transplants are performed annually [1], and considering the limited supply of donor organs, every effort is made to salvage the transplanted kidney [2]. However, acute rejection - the immunological response of the human immune system to the foreign kidney - is the most important cause of graft failure after renal transplantation, and the differential diagnosis of acute transplant dysfunction remains a difficult clinical problem.

Currently, the diagnosis of rejection is done via biopsy, but biopsy has the downside effect of subjecting the patients to risks like bleeding and infections. Moreover, the relatively small needle biopsies may lead to over or underestimation of the extent of inflammation in the entire graft [3]. Therefore, a noninvasive and repeatable technique is not only helpful but also needed in the diagnosis of acute renal rejection. For this purpose, detection of acute renal rejection after kidney transplantations has become an ongoing collaboration between the University of Mansoura and the CVIP Lab at the University of Louisville where Dynamic Contrast-Enhanced Magnetic Resonance Imaging (DCE-MRI) is applied prior to biopsy for its superior functional and anatomical information. In DCE-MRI, a contrast agent called Gd-DTPA is injected into the bloodstream, and as it perfuses into the organ, the kidneys are imaged rapidly and repeatedly. During the perfusion, Gd-DTPA causes a change in the relaxation times of the tissue and creates a contrast change in the images. As a result, the patterns of the contrast change gives functional information, while MRI provides good anatomical information which helps in distinguishing the diseases that affect different parts of the kidneys. However, even with an imaging technique like DCE-MRI, there are several problems; such as, (i) the spatial resolution of the dynamic MR images is low due to fast scanning, (ii) the images suffer from the motion induced by the breathing patient which necessitates advanced registration techniques, (iii) the intensity of the kidney changes non-uniformly as the contrast agent perfuse into the cortex which complicates the segmentation procedures.

To the best of our knowledge, there has been limited work on the dynamic MRI to overcome the problems of registration and segmentation. For the registration problem, Gerig et al.[7] proposed using Hough transform to register the edges in an image to the edges of a mask and Giele et al.[6] introduced a phase difference movement detection method to correct kidney displacements. Both of these studies required building a mask manually by drawing the kidney contour on a 2D DCE-MRI image, followed by the registration of the time frames to this mask.

For the segmentation problem, Boykov et al. [5] presented the use of graph cuts using Markov models; where the energy is minimized depending on the manually exerted seed points. Giele et al.[6] used image subtraction to obtain a mask, and closed the possible gaps by the use of a hull function. For further segmenting the medulla and the cortex structures, repeated erosions were applied to the mask to obtain several rings; however, in such rings, the medulla structures were intermixed with the cortex structures, so a correlation study had to be applied to better classify the cortical and medullary pixels.

Following these studies, a multi-step registration approach was introduced by Sun et al. [8]. Initially, the edges are aligned using an image gradient based similarity measure consider-

ing only translational motion. Once roughly aligned, a high-contrast image is subtracted from a pre-contrast image to obtain a kidney contour; which is then propagated over the other frames searching for the rigid registration parameters. For the segmentation of the cortex and medulla, a level sets approach was used.

2. METHODS

In this paper we introduce a novel and automated technique (i) to segment the kidney and (ii) to correct for the motion artifacts caused by breathing and patient motion; the details of which are given below.

2.1. Segmentation

Accurate segmentation of the kidney from DCE-MRI is a challenge since the gray level distribution of the kidney and surrounding organs is not highly distinguishable, thus we add additional constraints based on the shape of the objects to control the evolution of the deformable models in the segmentation process. So the proposed deformable model takes into account not only the gray level distribution but also a shape model of the kidney that depends on a sign distance map.

In conventional deformable models, surfaces move in the direction that minimizes an energy function that is composed of internal and external energy components given as:

$$E = E_{\text{int}} + E_{\text{ext}} = \int_{\tau \in T} \big(\xi_{\text{int}}\big(\phi(\tau)\big) + \xi_{\text{ext}}\big(\phi(\tau)\big)\big) d\tau \quad (1)$$

where $\xi_{\text{int}}\big(\phi(\tau)\big)$ and $\xi_{\text{ext}}\big(\phi(\tau)\big)$ denote the internal and external force, respectively.

Typical external forces designed in [9] lead a deformable model toward edges in a 2D grayscale image. This and the other traditional external forces (e.g. based on lines or, edges, or the gradient vector flow) fail to make the deformable model closely approach an intricate boundary with concavities. As a solution to this problem, we modify the external energy component of this energy formulation, and we formulate an energy function using the density estimations of two distributions: the signed distance map from shape models and the gray level distribution. The external energy component of our deformable models is formulated as:

$$\xi_{ext}\big(\phi(\tau)\big) = \begin{cases} -p(q|k)p_s(d|k)p(k) & \text{f} \quad k = k^* \\ \quad p(q|k)p_s(d|k)p(k) & \text{f} \quad k \neq k^* \end{cases}$$

In this formulation, k is the region label with $k = 1$ for the background and $k = 2$ for the kidney, q is the gray level, d is the signed distance; where $p_s(d|k)$ represents the density that describes the signed distance map inside and outside the object, and $p_g(q|k)$ is the density estimation of the gray level. With this energy function, the stochastic external force for each control point $\phi(\tau)$ of the current deformable model evolves in a region k^*. In this paper we used our previous probabilistic model to get accurate density estimation using linear combination of Gaussian (LCG) distribution with **positive** and **negative** components for both $p_g(q|k)$ and $p_s(d|k)$ [10].

The density of the signed distance map $p_s(d|k)$ in the above mentioned external energy is calculated using a shape model, which is basically an average shape obtained from the images in the data set.

A typical DCE–MRI scan of a kidney is given in Fig. 1(a), and the steps to estimate its gray level density are illustrated in Fig. 1(b,c,d). In Fig. 2(a) the average shape of a kidney obtained from 30 subjects is given with the signed distance map inside and outside the object as in Fig. 2(b); and its density estimation in (c). Finally, Fig. 3 shows the segmentation results of our approach compared to the segmentations by a radiologist.

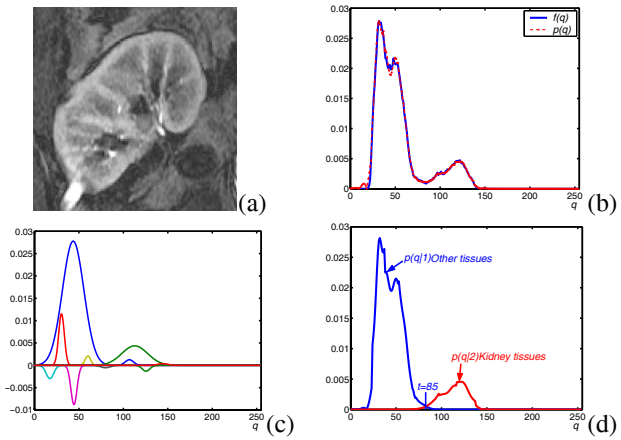

Fig. 1. Typical MRI scan of a kidney (a); and its gray level density estimation with the Modified EM Algorithm: (b) LCG components of the density estimation, (c) the final estimated density $p_g(q)$ (in red) for the empirical density $f(q)$ (in blue) of the kidney image, (d) the marginal density estimation for each class.

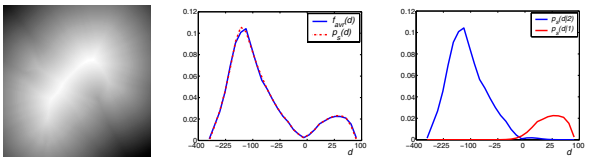

Fig. 2. (a) The average signed distance map inside and outside the kidney shape. (b) Density estimation $p_s(d)$ of the signed distance map density $f_{avr}(d)$. (c) Marginal density estimations for each class; red indicating the kidney and blue indicating the background.

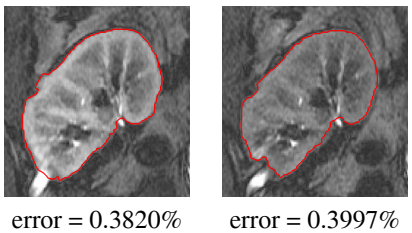

Fig. 3. Segmentation results using the proposed approach with the errors w.r.t the radiologist segmentation.

2.2. Model for the local deformation

In DCE-MRI sequences, the registration problem arises because of the patient & breathing movements. To overcome this problem, we proposed a new a approach to handle the kidney motion. The proposed approach is based on deforming the segmented kidney over closed equispaced contours (i.e. iso-contours) to closely match the prototype. We do not use a free-form deformation based on B-spline on square lattice because it requires additional smoothing constraints that lead to very time consuming computations. Instead we use evolution of the iso-contours guided with an exponential speed function in the directions minimizing distances between corresponding pixel pairs on the iso-contours of both the objects. The normalized cross-correlation is used as image similarity measure insensitive to intensity changes (e.g. due to tissue motion in medical imagery and the contrast agent).

The first step of the proposed approach is to use the fast marching level set methods [11] to generate the distance map inside the kidney regions as shown in Fig. 4(a), (b). The second step is to use this distance map to generate equal space separated contours (iso-contours) as shown in Fig. 4(c) and (d). Note that the number of iso-contours depend on the accuracy and the speed which the user needs to achieve. The third step of the proposed approach is to use normalized cross correlation to find the correspondence between the iso-contours. Since we start with aligned images, we limit our searching space to a small window (e.g. 10×10) to improve the speed of the proposed approach. The final step is the evolution of the iso-contours; here, our goal is to deform the iso-contours in the first image (target image) to match the iso-contours in the second image (source image). Before we discuss the details of the evolution algorithm lets define the following terminology:

- $\phi^A_{n_{iso}}(h,\nu)$ is the iso-contours in the target image, where $h = 1,\ldots,\mathcal{H}$ is the index of the control points in the given contour, $n_{iso} = 1,\ldots N_{iso}$ is the index of the iso-contours, and ν is the iteration step.
- $\phi^B_{m_{iso}}(\gamma)$ is the iso-contours in the source image, where $\gamma = 1,\ldots,$ is the index of the control points in the given contour, and $m_{iso} = 1,\ldots,M_{iso}$ is the index of the iso-contours.
- S is Euclidean distance between two corresponding points located on both iso-contours of both images.
- $S^A_{n_{iso},n_{iso}-1}$ is the Euclidian distance between $\phi^A_{n_{iso}}(l,\nu)$ and $\phi^A_{n-1}(l,\nu)$
- $\mathbf{V}$ is the propagation speed function.

The most important step in the model propagation is the selection of the propagation speed function $\mathbf{V}$. The selection of the speed function must satisfy the following conditions:

1. $\mathbf{V} = 0$ if $S = 0$
2. $\mathbf{V} \leq \quad (S, S^A_{n_{iso},n_{iso}-1}, S^A_{n_{iso},n_{iso}+1})$ if $S > 0$; is the smoothness constraint, which prevents the current point from passing the closest neighbor contour as shown in Fig. 5.

The speed function of the following form satisfies the above conditions:

$$\mathbf{V} = e^{\beta S} - 1 \tag{2}$$

where β is the propagation constant with the upper bound

$$\beta \preceq \frac{\left(\quad (S, S^A_{n_{iso},n_{iso}-1}, S^A_{n_{iso},n_{iso}+1}) + 1 \right)}{S}$$

Based on the speed function shown in Eq. (2) we can deform the iso-contours using the following equation as shown in Fig. 5(b):

$$\phi^A(h,\nu+1) = \tfrac{\mathbf{V}}{S}\phi^B_{m_{iso}}(\gamma) + \tfrac{S-\mathbf{V}}{S}\phi^A_{n_{iso}}(h,\nu) \tag{3}$$

for $h = 1,\ldots,\mathcal{H},\ m_{iso} = 1,\ldots,M_{iso},\ n_{iso} = 1,\ldots,N_{iso}$.

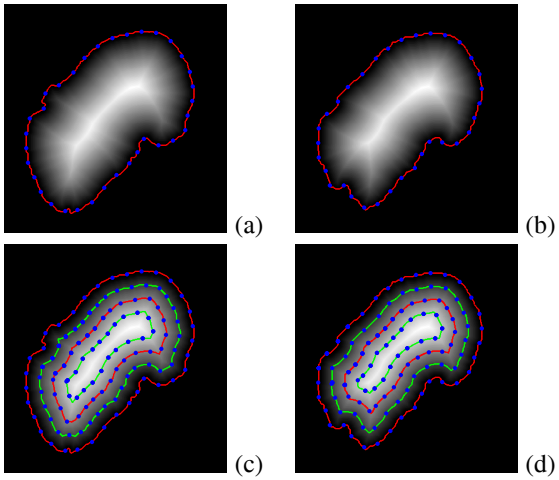

Fig. 4. The distance map of two kidneys (a, b) and the isocontours (c, d).

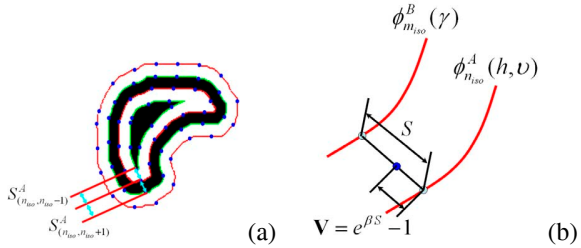

Fig. 5. (a) Model constrains and (b) model evolution.

The final step of our approach is to segment the cortex from the segmented kidney. To achieve this task, we use the same approach but based only on the intensity. In Fig. 7, we show the cortex segmentation results on two of the kidneys.

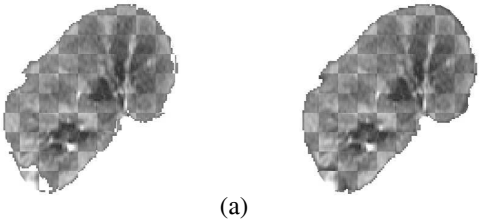

(a) (b)

Fig. 6. Checkerboard image to show the quality of the approach, (a) before non-rigid registration, and (b) after non-rigid registration.

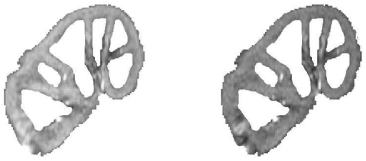

Fig. 7. The segmentation of the cortex from the kidney images.

3. RESULTS AND CONCLUSION

The ultimate goal of the proposed algorithms is to successfully construct a renogram (mean intensity signal curves) from the DCE-MRI sequences, showing the behavior of the kidney as the contrast agent perfuse into the transplant. In acute rejection patients, the DCE-MRI images show a delayed perfusion pattern and a reduced cortical enhancement. We tested the above algorithms on thirty patients; four of which are shown in Figure 8. The normal patient shows the expected abrupt increase to the higher signal intensities and the valley with a small slope. The acute rejection patients show a delay in reaching their peak signal intensities. From these observations, we have been able to conclude that the relative peak signal intensity, time to peak signal intensity, the slope between the peak and the first minimum, and the slope between the peak and the signal measured from the last image in the sequence are the major four features in the renograms of the segmented kidney for classification.

To distinguish between normal and acute rejection, we use Bayesian supervised classifier learning statistical characteristics from a training set for the normal and acute rejection. The density estimation required in the Bayes classifier is performed for each feature by using a linear combination of Gaussians (LCG) with positive and negative components, their parameters are estimated using a modified EM algorithm which appeared in [10]. In our approach we used 50% of the data for the training and the other 50% for testing. For testing data, the Bayes classifier succeeds to classify 13 out of 15 correctly (86.67%). For the training data the Bayes classifier classifies all of them correctly, so the over all accuracy of the proposed approach is 93.3%.

In this paper we presented a framework for the detection of acute renal rejection from Dynamic Contrast Enhanced Magnetic Resonance Images which includes segmentation of the kidneys from the abdomen images, non-rigid registration and Bayes classification.

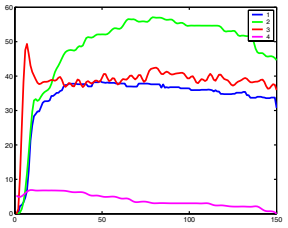

Fig. 8. Normalized cortex signals from 4 subjects wrt. scan number. Subjects 1 and 2 are acute rejection, subject 3 is normal and subject 4 is chronic glomerulopathy proved by biopsy.

4. REFERENCES

[1] U.S. Department of Health and Human Services. Annual report of the U.S. scientific registry of transplant recipients and the organ procurement and transplantation network: transplant data: 1990-1999. Bureau of Health Resources Department, Richmond, VA; 2000.

[2] M. Neimatallah *et al.*, "Magnetic resonance imaging in renal transplantation, J Magn Reson Imaging, vol. 10(3), pp. 357-368, Sep 1999.

[3] D. Yang *et al.*, "USPIO-Enhanced Dynamic MRI: Evaluation of Normal and Transplanted Rat Kidneys," Magn. Reson. in Medicine, vol. 46, 1152-1163, 2001.

[4] P.L. Choyke *et al.*, "Dynamic Gd-DTPA-Enhanced MR imaging of the kidney: experimental results," Radiology 1989; 170:713-720

[5] Y. Boykov *et al.*, "Segmentation of dynamic N-D data sets via graph cuts using Markov models," in Proc. of MICCAI, 2001, pp. 1058-1066.

[6] E. Giele, "Computer methods for semi-automatic MR renogram determination," Ph.D. dissertation, Department of Electrical Engineering, Eindhoven University of Technology, Eindhoven, 2002.

[7] G. Gerig *et al.*,"Semiautomated ROI analysis in dynamic MRI studies: Part I: image analysis tools for automatic correction of organ displacements," IEEE Trans. Image Processing, Vol. 11:(2),pp. 221-232, 1992.

[8] Y. Sun *et al.*, "Integrated Registration of Dynamic Renal Perfusion MR Images," in Proc. of ICIP'04,pp. 1923–1926, 2004.

[9] M. Kass *et al.*,"Snakes: Active contour models," *International Journal of Computer Vision*, vol. 1, pp. 321–331, 1987.

[10] A. A. Farag *et al.*,"Density Estimation Using Modified Expectation-Maximization for a linear combination of Gaussians," *in Proc. IEEE Int. Conf. Image Processing (ICIP 2004)*, Singapore, October 2004. in Proc. ICIP 2004, Singapore, October 2004.

[11] J. A. Sethian, "Fast marching level set method for monotonically advancing fronts," *Proc. Nat. Acad. Sci. USA*, vol. 93, pp. 1591-1595, Feb. 1996.